Large magnetic penetration depth and thermal fluctuations in a $Ca_{10}(Pt_3As_8)[(Fe_{1-x}Pt_x)_2As_2]_5$ (x=0.097) single crystal

Jeehoon Kim,[1] Filip Ronning,[1] N. Haberkorn,[1] L. Civale,[1] E. Nazaretski,[2] Ni Ni,[3] R. J. Cava,[3] J. D. Thompson,[1] and R. Movshovich[1]

[1]*Los Alamos National Laboratory, Los Alamos, NM 87545**
[2]*Brookhaven National Laboratory, Upton, NY 11973*
[3]*Department of Chemistry, Princeton University, Princeton, NJ 08544*

(Dated: March 4, 2013)

We have measured the temperature dependence of the absolute value of the magnetic penetration depth $\lambda(T)$ in a $Ca_{10}(Pt_3As_8)[(Fe_{1-x}Pt_x)_2As_2]_5$ (x=0.097) single crystal using a low-temperature magnetic force microscope (MFM). We obtain $\lambda_{ab}(0)\approx$1000 nm via extrapolating the data to $T = 0$. This large λ and pronounced anisotropy in this system are responsible for large thermal fluctuations and the presence of a liquid vortex phase in this low-temperature superconductor with critical temperature of 11 K, consistent with the interpretation of the electrical transport data. The superconducting parameters obtained from λ and coherence length ξ place this compound in the extreme type II regime. Meissner responses (via MFM) at different locations across the sample are similar to each other, indicating good homogeneity of the superconducting state on a sub-micron scale.

Iron-based superconductors offer an opportunity to explore superconductivity over a very wide range of superconducting properties, such as critical fields, superfluid densities, and their anisotropy.[1] Comparing iron-based superconductors with cuprates provides clues to the mechanism of high T_c superconductivity that determine fundamental superconducting parameters, such as the gap symmetry[2,3] and the upper critical fields,[4] as well as complex vortex dynamics due to the thermal fluctuations.[5–7] Understanding the correlation between intrinsic properties and the pinning mechanism is thus intriguing from both basic and applied points of view. Recently, superconductivity has been reported in a new family of highly anisotropic materials; $Ca_{10}(Pt_nAs_8)[(Fe_{1-x}Pt_x)_2As_2]_5$ (Ca-Pt-Fe-As) with n=3 ("10-3-8") and n=4 ("10-4-8").[8–10] The 10-3-8 phase has *triclinic* symmetry and a T_c of up to 11 K upon Pt doping; the 10-4-8 phase has tetragonal symmetry with the highest T_c of 38 K. It is worth noting that well-defined Fermi surface sheets with tetragonal symmetry, similar to other pnictides, are observed in the 10-3-8 phase in spite of its triclinic symmetry.[11] Anisotropy of the critical field in the 10-3-8 phase near T_c, $\gamma_{H_{c2}}(T_c) \equiv H_{c2}^{ab}/H_{c2}^{c} \approx 10$ (Ref. 8), is much larger than that of the 122 pnictide compounds, $\gamma_{H_{c2}}(T_c) \approx 2$ (Ref. 12), consistent with a more anisotropic 2D nature of the 10-3-8 system. In contrast to $Ba(Fe_{1-x}Co_x)_2As_2$ superconductors, well-studied by a variety of techniques,[13] 10-3-8 shows a broadened superconducting transition temperature with applied field,[8] consistent with strong thermal fluctuations of vortices.[5]

In this Rapid Communication we present measurements of the absolute value of the magnetic penetration depth λ in the 10-3-8 compound. We derive the values of several basic superconducting parameters from our measurements and relate them to other unusual properties observed in the 10-3-8 compound, such as a broadened superconducting phase transition. We have determined the temperature dependence of the absolute value of $\lambda(T)$ in a 10-3-8 single crystal (x=0.097)[8] with $T_c \approx 11$ K using a Meissner technique employing magnetic force microscopy (MFM). Our experimental approach for λ measurements is simple, robust, and independent of the MFM tip model whereas most previous MFM studies provided either $\delta\lambda$ variations or the absolute value from modeling the tip magnetization instead of measuring λ directly.[14,15] Recently, the temperature dependence of $\delta\lambda$ was measured via a tunnel-diode resonator technique, and it showed an increasing anisotropy of the superconducting gap as doping decreases from optimal doping towards the edges of the superconducting dome.[16] Our MFM results show that the superconductivity is homogeneous, which agrees well with tunnel diode,[16] transport,[8] and angle resolved photoemission spectroscopy (ARPES) data.[11] By extrapolating our temperature dependent data from 4 K to $T = 0$, we obtain $\lambda_{ab}(0)\approx$1000 nm. The short electron mean free path in this system, compared to the coherence length, suggests that this system is in the dirty limit, which is partly responsible for the large λ value. Strong thermal fluctuations inferred from the Ginzburg number are consistent with a wide superconducting transition under field and the presence of a vortex-liquid phase in this highly anisotropic superconductor with relatively *low* T_c.[8]

Synthesis of the 10-3-8 system is described elsewhere.[8] All measurements described here were performed in a home-built low-temperature MFM apparatus,[17] which allows acquisition of a complete set of MFM data on several samples with identical MFM tip conditions. With this apparatus, a Meissner response curve[14] is measured first as a function of the tip-sample separation in the reference sample (Nb film), and then, the cantilever is moved to the sample of interest (10-3-8) where its Meissner response as a function of tip-sample distance is obtained. Direct comparison of these curves yields the absolute value of λ_{ab} in 10-3-8 and its temperature dependence $\lambda_{ab}(T)$. (We measure λ_{ab} since the shielding currents run in the

basal plane.) The λ value of the reference Nb film was verified by both a different MFM technique and SQUID magnetometry measurements, as described elsewhere.[15] The vortex imaging, after field-cooling the sample in a field of a few Oersted to avoid the demagnetization effect of the sample, was performed in a frequency modulation mode with the tip-lift height of 400 nm above the sample surface. The zero point of the tip-sample separation was determined by touching the surface of the sample; this touchdown of the tip resulted in a substantial negative frequency shift. The tip-sample separation was measured based on the calibration of the piezo scanner. We used a high resolution cobalt-coated Nanosensors cantilever[18] that was polarized along the tip axis in a 30-kOe magnetic field (H). The Meissner experiment was performed under the conditions of no vortices being present in a 20 μm $\times$ 20 μm field of view, which eliminates possible force contributions of vortices to the Meissner force. Before vortex measurements on the 10-3-8 sample, the stray field (H_{sf}) from a superconducting magnet was calibrated by measuring the number of vortices as a function of field on the Nb reference (see Fig. 1(b)): the Nb reference serves as a magnetic field sensor. The red line in Fig. 1(b) is a linear fit to the experimental data with a fit function of $N = (N/H)H + H_{sf}$, where N is a number of vortices. The obtained slope and H_{sf} from the fit are 1.6 Oe^{-1} and -2.6 Oe, respectively. The calculated single vortex flux Φ_{exp} from the slope of the fit and the area of a vortex image is $\Phi_{exp} = area \times (N/H)^{-1} = (6\ \mu\text{m} \times 6\ \mu\text{m}) \times (1.6)^{-1} = 22.6\ \text{G}\mu\text{m}^2$, which is in good agreement with the theoretical value of a single flux quantum $\Phi_0 = h/2e = 20.7\ \text{G}\mu\text{m}^2$. The Nb reference film is homogeneous with a uniform (though irregular) distribution of vortices. The stray field calibration in panel (b) in Fig. 1 was reproducible at 3 different locations of the Nb reference.

Figs. 1(c)-(f) show MFM images obtained at two different nominal fields of $H = -3$ Oe and $H = -7$ Oe in both the Nb reference (panels (c) and (d)) and the 10-3-8 single crystal (panels (e) and (f)). We obtained MFM images at several locations across the sample's surface separated by hundreds of microns and observed no vortices. Thermal drift of the MFM system equals a few nanometers per hour at 4 K. The low drift comes from a rigid design of the MFM apparatus. More technical details can be found in Ref. 15. This indicates that the lack of vortices in a 10-3-8 sample is an intrinsic property. The lack of vortices may be due to a large λ, leading to a very slow exponential decay of the vortex profile over a large length scale, and hence a smaller intensity of the MFM signal in the vortex center.[19] To verify this possibility, we measured the Meissner response as a function of the tip-sample separation. An MFM tip experiences a Meissner force because of the interaction between the tip magnetic moment and a field generated from the shielding current induced by the tip moment. The Meissner response force can be expressed as a function of λ and the tip-sample separation d, $F_{Meissner} = A \times f(d + \lambda)$,

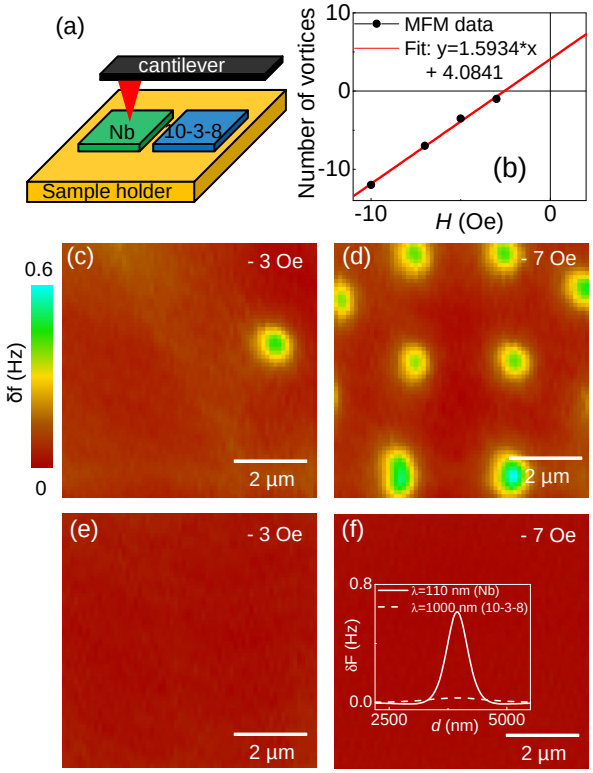

FIG. 1: (Color online) (a) Schematic illustration of our sample holder with multiple samples. A Nb thin film (300 nm) and a 10-3-8 single crystal are located next to each other. (b) The number of vortices as a function of the magnetic field. The red (light gray) line represents a linear fit to the experimental data. (c) and (e) MFM images of the Nb sample and the 10-3-8 sample taken at T =4 K in H =-3 Oe, respectively. (d) and (f) The same type of MFM images as in (c) and (e) but with H =-7 Oe. No individual vortices were clearly resolved in 10-3-8 due to a large λ ((e) and (f)) as opposed to the Nb reference. The color scale bar is applied for (c)-(f). The inset in panel (f) shows a simulation of the expected frequency shift for two different λ values. The solid line represents a calculated line profile for Nb and the dashed curve shows a profile for a 10-3-8 sample based on the monopole-monopole interaction between the tip and the sample. The frequency shift of the vortex center in a 10-3-8 sample is around 30 mHz (close to the noise level). Small frequency shift prevents visualization of vortices.

where A is a prefactor that reflects the sensor's geometry and the magnetic moment.[14,20–23] The Meissner forces obtained from a Nb reference and the 10-3-8 sample have the same functional form, $F^{Nb}(d) = A \times f(d + \lambda_{Nb})$ and $F^{10-3-8}(d) = A \times f(d + \lambda_{10-3-8})$, respectively. Note that A and f are the same in both cases when the tip is at the same condition. As a result, $\lambda_{10-3-8} = \lambda_{Nb} + \delta\lambda$, where the reference $\lambda_{Nb} = 110$ nm has been previously determined[15] and $\delta\lambda$ is the shift required to overlay the $F(d)$ curves.

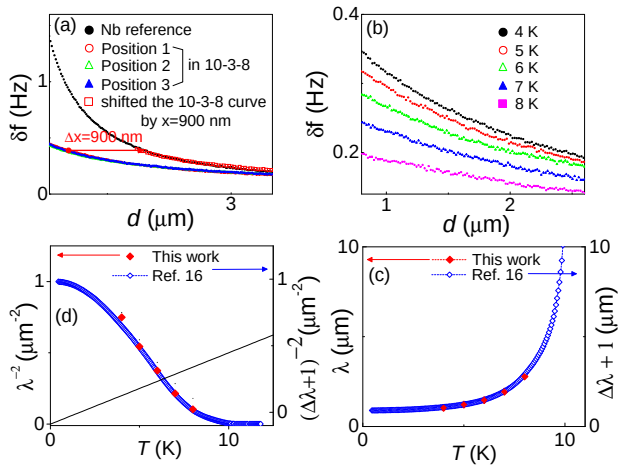

FIG. 2: (Color online) (a) Meissner curves obtained from a Nb reference and a 10-3-8 sample with the same experimental conditions during a single cool-down. The Meissner curves obtained from 10-3-8 were obtained at three lateral positions separated by approximately 10 μm. Their similarity indicates good homogeneity of the superconducting state on a sub-micron scale in the sample. By shifting the red empty curve by 900 nm, the resulting curve (red empty squares) overlays the Nb reference curve. (b) Temperature dependent Meissner response curves. Note that the Meissner curves decay more slowly with increasing tip-sample separation as the temperature increases, indicating an increase of λ with temperature. (c) Temperature dependent λ measurements. Red filled diamonds are experimental data inferred from curves in Fig. 2(b). Blue empty diamonds are taken from tunnel diode resonator measurements.[16] We shifted tunnel diode data along the y axis by 1 μm, the value obtained from MFM measurements and overlaid on our data to directly compare with the MFM data. (d) Superfluid density $\rho_s(T)$ calculated from Fig. 2(c). The black line corresponds to $\rho_s^{2D} \equiv \hbar^2 d/4k_B e^2 \mu_0 \lambda^2 = (2/\pi)T$ in each FeAs plane.

Fig. 2(a) shows Meissner curves obtained from the Nb film and the 10-3-8 single crystal. The Meissner curves in the 10-3-8 sample were obtained at three lateral positions separated by approximately 10 μm: the uniformity of the curves indicates that λ is homogeneous on a sub-micron scale. As opposed to the Nb reference, the Meissner curve for the 10-3-8 crystal decays slowly as the tip-sample separation increases, indicating the λ for the 10-3-8 compound is larger than that of Nb. The absolute value of λ in the 10-3-8 sample is obtained by offsetting the 10-3-8 Meissner curve to overlay the response in the Nb reference. The offset yields $\delta\lambda$ of 900 nm, as shown by the arrow in Fig. 2(a), and therefore $\lambda_{10-3-8} = 1000 \pm 100$ nm. The temperature-dependent penetration depth, shown in Fig. 2(c), was obtained from Meissner curves measured at different temperatures, as shown in Fig. 2(b). Fig. 2(c) displays the absolute values of of $\lambda(T)$ obtained using MFM (red filled diamonds) and using tunnel diode measurements[16] (blue empty diamonds). To compare the two data sets, the tunnel diode data ($\delta\lambda(T)$) are shifted along the y axis by 1 μm, the absolute value of $\lambda(0)$ obtained from MFM measurements. These data sets demonstrate consistency, proving the validity of the MFM approach. We also measured the absolute value of λ in a 10-3-8 sample with a different doping level ($x = 0.042$; $T_c \approx 10$ K) and obtained (a doping dependence) $\lambda_{ab}(0) \approx 1200\pm100$ nm.

The large λ measured here can be due to either impurity scattering or an intrinsically small superfluid density. To evaluate the contribution from impurities, we first estimate the electronic mean free path using the Drude model: $l = \frac{1}{2\pi}\frac{R_K k_F}{n\rho}$, where R_K is the von Klitzing constant ($R_K = h/e^2 \approx 25813\ \Omega$), k_F is the Fermi wave vector, n is the charge carrier density, and ρ is the resistivity. We obtain $l \approx$1.5 nm, using n and ρ obtained via transport measurements[8] and $k_F \approx 0.3\pi/a$ from ARPES[10]. The mean free path (l = 1.5 nm) is shorter than the coherence length (ξ = 5 nm) obtained from transport[8] ($l < \xi$), and indicates that the system is in the dirty limit, partially explaining the large λ value. In the dirty limit the effective penetration depth is $\lambda_{eff}(0) = \lambda_{clean}(0)(1 + \xi_0(0)/l)^{1/2}$ using the local approximation and the effective coherence length is $\xi_{eff} = \xi_{clean}(0)/(1 + \xi_0(0)/l)^{1/2}$.[24,25] For ξ_0 =19.7 nm (obtained from the equation of ξ_{eff}), λ_{eff} =1000 nm, and l =1.5 nm, λ_{clean} in the clean limit is approximately 270 nm.

A large λ also can be due to a small superfluid density. The London penetration depth $\lambda_L = \sqrt{\frac{m^\star}{\mu_0 n e^2}}$, where $m^\star$ is an effective electron mass, μ_0 is the vacuum permeability, n is the charge carrier density, and e is an electron charge. ARPES E(k) data allow us to calculate the effective mass of the charge carriers using the expression $1/m^\star = \frac{1}{\hbar^2}(d^2E/dk^2)_{E_f}$. We obtain $m^\star \approx 7.3 m_e$, where m_e is a bare electron mass[10]. This $m^\star$ and $n \approx 0.74 \times 10^{27}$ m^{-3}, obtained from transport measurements,[8] results in $\lambda_L \approx 530$ nm. This calculated λ_L corresponds to an intrinsic λ, because the experimental band dispersion and carrier density do not depend on disorder. Therefore, we can directly compare $\lambda_{clean} \approx 270$ nm with $\lambda_L \approx 530$ nm from ARPES and transport. The discrepancy is likely a result of the carrier density being obtained using a single band approximation; whereas, ARPES and theoretical electron band calculations show a multiband character of the Fermi surface.

The small superfluid density, reflected in the large measured penetration depth, indicates a weak phase stiffness of the superconducting order parameter and suggests that phase fluctuations may be important in 10-3-8. We add in Fig. 3 the values of λ for 10-3-8 as red filled stars to the Uemura plot,[26] which shows the scaling between $\lambda^{-2}(0) \propto n_s/m^\star$ and T_c in unconventional superconductors. We see that the phase stiffness relative to T_c is weaker than in other Fe-based superconductors as well as the cuprates, even weaker than that in highly underdoped

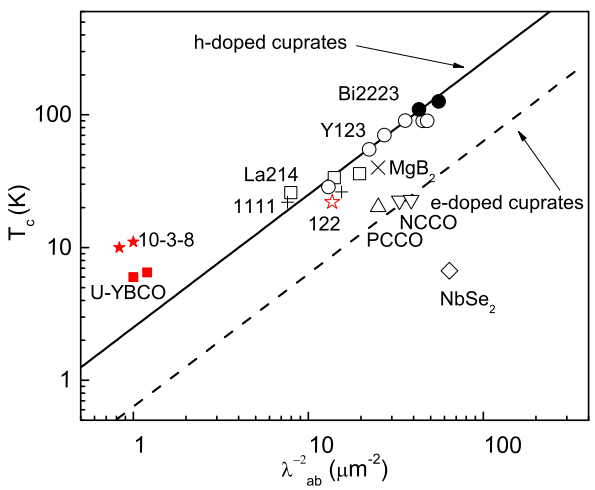

FIG. 3: (Color online) Uemura plot for high T_c cuprates. The data for the cuprates and points for the 1111 system are taken from Ref. 27. The data for MgB_2 and $NbSe_2$ are taken from Ref. 28 and Ref. 29, respectively. The red filled squares show highly underdoped YBCO superconductors taken from Ref. 30. The red filled stars represent the data for 10-3-8 obtained in this work.

YBCO.[27,30,31] This may reflect a "Swiss cheese" like response of the system to impurities, indicating nanoscale inhomogeneity is likely present in 10-3-8.[32,33] Our measurement of λ is not sensitive to heterogeneity on this scale. The relatively large anisotropy of the upper critical field further suggests that 10-3-8 may be the most quasi-2D material of all Fe-based superconductors,[8] thus bearing more resemblance to the cuprate superconductors. Fig. 2(d) shows the measured superfluid density $\rho_s(T)$ as well as prediction of the Kosterlitz-Thouless-Berezinsky (KTB) theory of vortex-unbinding that should be applicable to a highly anisotropic 2D superconductor.[34] $\rho_s(T)$ passes smoothly through the KTB line, indicating that superconductivity of the 10-3-8 phase is still of a 3-D character.

We now discuss the effects of the large λ on other superconducting properties. The H_{c2} values obtained from the Werthamer-Helfand-Hohenberg theory[35] are $H_{c2}^{\parallel ab} = 55$ T and $H_{c2}^{\perp ab} = 13$ T, and the corresponding ξ values are $\xi_{\parallel ab}(0) = 5$ nm and $\xi_{\perp ab}(0) = 1.2$ nm.[8] We calculate $\kappa = \lambda_{ab}/\xi_{ab} \approx 200$, using $\lambda_{ab} \approx 1000$ nm and $\xi_{ab} \approx 5$ nm, the thermodynamic critical field $H_c = \Phi_0/2\sqrt{2}\pi\lambda(0)\xi(0) \approx 500$ Oe, and the depairing current $J_d = \Phi_0/3\sqrt{3}\pi\mu_0\lambda^2\xi \approx 2$ MAcm^2. These values indicate that the 10-3-8 compound is an extreme type II superconductor. Anisotropy of the critical field in this compound $\gamma_{H_{c2}} = H_{c2}^{\parallel ab}/H_{c2}^{\perp ab}$ shows a strong temperature dependence, ranging from 10 near T_c to 5 at $0.9T_c$.[8] The resistive signature of the superconducting transition broadens with increasing magnetic field, indicating the presence of strong magnetic fluctuations.[8] The fundamental parameter governing the strength of the thermal fluctuations is the Ginzburg number Gi, $Gi = [T_c\gamma/H_c^2(0)\xi^3(0)]^2/2$, where H_c is the thermodynamical critical field and γ is the anisotropy parameter.[5] Using $T_c \approx 11$ K, $\gamma \approx 10$, $\xi = 5$ nm, and $\lambda \approx 1000$ nm, we obtain $Gi \approx 0.16$. The theoretical width of the transition, $\Delta T_c \geq Gi \cdot T_c$, is approximately 1.8 K, consistent with the experimental value of $\Delta T_c \approx 2$ K; although, we can not rule out that the rounding is also partially a result of nanoscale spatial inhomogeneity of T_c.[8] The Gi in the 10-3-8 compound is larger than that in YBCO (Gi =0.01) and BiSCCO (Gi =0.1).[5] The broadening of the superconducting transition with increasing magnetic field is consistent with the presence of a vortex-liquid phase, similar to cuprates.[5]

In conclusion, we measured the absolute value of λ in a single crystal of $Ca_{10}(Pt_3As_8)[(Fe_{1-x}Pt_x)_2As_2]_5$ (x=0.097) using a Meissner technique in a low temperature MFM apparatus. Similar Meissner responses in different regions of the sample indicate that the superconductivity is homogeneous on a scale of λ. We obtain the value of $\lambda(0)$ in our sample of approximately 1000 nm. The clean limit penetration depth is calculated to be 270 nm based on an impurity scattering model. The large Ginzburg number ($Gi \approx 0.16$) agrees well with the previously reported data that show a broad superconducting transition and a signature of a vortex liquid phase in this highly anisotropic *low* $T_c = 11$ K superconductor.

We acknowledge valuable discussions with M. Graf. Work at Los Alamos was supported by the US Department of Energy, Office of Basic Energy Sciences, Division of Materials Sciences and Engineering. Work at Brookhaven was supported by the US Department of Energy under Contract No. DE-AC02-98CH10886. Work at Princeton was supported by the AFOSR MURI on superconductivity, grant FA9550-09-1-0593. We thank K. Cho, M. Tanatar, and R. Prozorov for supplying data from Ref. 16. N. H. is member of CONICET, Argentina.

* Corresponding author: jeehoon@lanl.gov

[1] J. Paglione and R. L. Greene, Nat. Phys. **6**, 645 (2000).
[2] Yi Yin, M. Zech, T. L. Williams, X. F. Wang, G. Wu, X. H. Chen, and J. E. Hoffman. Phys. Rev. Lett. **102**, 097002 (2009).
[3] A. V. Chubukov, M. G. Vavilov, and A. B. Vorontsov. Phys. Rev. B **80**, 140515 (2009).
[4] H. Q. Yuan, J. Singleton, F. F. Balakirev, S. A. Baily, G. F. Chen, J. L. Luo, and N. L. Wang, Nature **457**, 33 (2009).
[5] G. Blatter, M.V. Feigel′man, V.B. Geshkenbein, A.I. Larkin and V.M. Vinokur, Rev. Mod. Phys. **66** 1125 (1994).
[6] R. Prozorov, N. Ni, M. A. Tanatar, V. G. Kogan, R. T. Gordon, C. Martin, E. C. Blomberg, P. Prommapan, J. Q.

Yan, S. L. Bud'ko, and P. C. Canfield, Phys. Rev. B **78**, 224506 (2008).
[7] C. J. van der Beek, G. Rizza, M. Konczykowski, P. Fertey, I. Monnet, Thierry Klein, R. Okazaki, M. Ishikado, H. Kito, A. Iyo, H. Eisaki, S. Shamoto, M. E. Tillman, S. L. Bud'ko, P. C. Canfield, T. Shibauchi, and Y. Matsuda, Phys. Rev. B **81**, 174517 (2010).
[8] Ni Ni, Jared M. Allred, Benny C. Chan, and Robert Joseph Cava, PNAS **108**, E1019 (2011).
[9] S. Kakiya, K. Kudo, Y. Nishikubo, K. Oku, E. Nishibori, H. Sawa, T. Yamamoto, T. Nozaka, and M. Nohara, J. Phys. Soc. Japan **80**, 093704 (2011).
[10] C. Löhnert, T. Stürzer, M. Tegel, R. Frankovsky, G. Friederichs, and D. Johrendt, Angew. Chem. Int. Ed., **50**, 9195 (2011).
[11] M. Neupane, C. Liu, S.-Y. Xu, Y. J. Wang, N. Ni, J. M. Allred, L. A. Wray, H. Lin, R. S. Markiewicz, A. Bansil, R. J. Cava, M. Z. Hasan, e-print arXiv:1110.4687v1 (2011).
[12] A. Gurevich, Rep. Prog. Phys. **74** 124501 (2011).
[13] N. Ni, M. E. Tillman, J.-Q. Yan, A. Kracher, S. T. Hannahs, S. L. Budko, and P. C. Canfield, Phys. Rev. B **78**, 214515 (2008).
[14] L. Luan, O. M. Auslaender, T. M. Lippman, C. W. Hicks, B. Kalisky, J. H. Chu, J. G. Analytis, I. R. Fisher, J. R. Kirtley, and K. A. Moler, Phys. Rev. B **81**, 100501(R) (2010).
[15] E. Nazaretski, J. P. Thibodaux, I. Vekhter, L. Civale, J. D. Thompson, and R. Movshovich, Appl. Phys. Lett. **95**, 262502 (2009).
[16] K. Cho, M. A. Tanatar, H. Kim, W. E. Straszheim, N. Ni, R. J. Cava, and R. Prozorov, Phys. Rev. B **85**, 020504(R) (2012).
[17] E. Nazaretski, K. S. Graham, J. D. Thompson, J. A. Wright, D. V. Pelekhov, P. C. Hammel, and R. Movshovich, Rev. Sci. Instrum. **80**, 083704 (2009).
[18] A SSS-QMFMR cantilever, Nanosensors, Inc, www.nanoandmore.com/USA/AFM-Probe-SSS-QMFMR.html.
[19] The maximum force gradient at the center of a vortex, $\max(\partial f/\partial z)$ (MFM is sensitive to a force gradient), is proportional to $(z+\lambda_{ab})^{-1/3}$ for a monopole-monopole model of the tip-vortex interaction. In this model, the larger value of λ results in a smaller force gradient at the center of a vortex.
[20] O. M. Auslaender, L. Luan, E. W. J. Straver, J. E. Hoffman, N. C. Koshnick, E. Zeldov, D. A. Bonn, R. Liang, W. N. Hardy, and K. A. Moler, Nature Phys., **5** 35 (2009).
[21] E. W. J. Straver, J. E. Hoffman, O. M. Auslaender, D. Rugar, and Kathryn A. Moler, Appl. Phys. Lett. **93**, 172514 (2008).
[22] Lan Luan, Ophir M. Auslaender, Nadav Shapira, Douglas A. Bonn, Ruixing Liang, Walter N. Hardy, Kathryn A. Moler, e-print arXiv:1103.6072v1.
[23] T. Shapoval, H. Stopfel, S. Haindl, J. Engelmann, D. S. Inosov, B. Holzapfel, V. Neu, and L. Schultz, Phys. Rev. B **83**, 214517 (2011).
[24] M. Tinkham, *Introduction to Superconductivity* (McGraw Inc., NY, 1975).
[25] T. K. Kim, A. N. Yaresko, V. B. Zabolotnyy, A. A. Kordyuk, D. V. Evtushinsky, N. H. Sung, B. K. Cho, T. Samuely, P. Szabó, J. G. Rodrigo, J. T. Park, D. S. Inosov, P. Samuely, B. Büchner, and S. V. Borisenko, Phys. Rev. B **85**, 014520 (2012).
[26] Y. J. Uemura, G. M. Luke, B. J. Sternlieb, J. H. Brewer, J. F. Carolan, W. N. Hardy, R. Kadono, J. R. Kempton, R. F. Kiefl, S. R. Kreitzman, P. Mulhern, T. M. Riseman, D. Ll. Williams, B. X. Yang, S. Uchida, H. Takagi, J. Gopalakrishnan, A. W. Sleight, M. A. Subramanian, C. L. Chien, M. Z. Cieplak, Gang Xiao, V. Y. Lee, B. W. Statt, C. E. Stronach, W. J. Kossler, and X. H. Yu, Phys. Rev. Lett. **62**, 2317 (1989).
[27] H. Luetkens, H.-H. Klauss, R. Khasanov, A. Amato, R. Klingeler, I. Hellmann, N. Leps, A. Kondrat, C. Hess, A. Köhler *et al.*, Phys. Rev. Lett. **101**, 097009 (2008).
[28] Jeehoon Kim *et al.*, unpublished.
[29] J. D. Fletcher, A. Carrington, P. Diener, P. Rodiere, J. P. Brison, R. Prozorov, T. Olheiser, and R. W. Giannetta, Phys. Rev. Lett. **98**, 057003 (2007).
[30] D. M. Broun, W. A. Huttema, P. J. Turner, S. Özcan, B. Morgan, R. Liang, W. N. Hardy, and D. A. Bonn, Phys. Rev. Lett. **99**, 237003 (2007).
[31] Yuri Zuev, Mun Seog Kim, and Thomas R. Lemberger, Phys. Rev. Lett. **95**, 137002 (2005).
[32] M. Franz, C. Kallin, A. J. Berlinsky, and M. I. Salkola, Phys. Rev. B **56**, 7882 (1997).
[33] T. Das, J. X. Zhu, and M. J. Graf, Phys. Rev. B **84**, 134510 (2011).
[34] J. M. Kosterlitz and D. J. Thouless, J. Phys. C **6**, 1181 (1973); V. L. Berezinskii, Sov. Phys. JETP **32**, 493 (1971).
[35] N. R. Werthamer, E. Helfand, and P. C. Hohenberg, Phys. Rev. **147**, 295 (1966).